Simulation of the Earth's Monthly Average Regional Radiation Balance Derived from Satellite Measurements

DAVID R. BROOKS AND PATRICK MINNIS

Atmospheric Sciences Division, NASA Langley Research Center, Hampton, VA 23665

(Manuscript received 29 March 1983, in final form 21 December 1983)

ABSTRACT

Computer simulations of satellite-derived Earth radiation parameters are examined to determine the source and size of errors arising from averaging parameters over 1 month on a 2.5° × 2.5° longitude–latitude grid. November 1978 data from the Geostationary Operational Environmental Satellite (GOES) have been used as a source of radiation parameter fields within each region. The regions are sampled according to various combinations of satellite orbits which have been chosen on the basis of their applicability to the Earth Radiation Budget Experiment. A mathematical model is given for the data-processing algorithms that are used to produce daily, monthly and monthly hourly estimates of shortwave, longwave and net radiant exitance. Because satellite sampling of each region is sparse during any day, and because the meteorological behavior between measurements is unknown, the retrieved diurnal cycle in shortwave radiant exitance is especially sensitive to the temporal distribution of measurements. The resulting retrieval errors are seen to be due to insufficient knowledge of the temporal distribution of both cloud fraction and albedo. These errors, in combination with similar sampling errors resulting from diurnal variations in longwave radiant exitance (especially over land), produce biases in monthly net radiant exitance which are complex, regionally-dependent functions of the local time of the measurements. The regions studied have shown standard errors of estimate for monthly net radiant exitance ranging from about 20 W m^{-2} for the worst single-satellite sample to ~2 W m^{-2} for the three-satellite sampling assumed to be available.

1. Introduction

The goal of satellite-based measurements of the Earth's radiation is to determine the Earth's radiation budget on regional, zonal (latitude bands), and global scales over monthly, seasonal and yearly time periods. There already exists a more than 20-year history of satellite-based radiation measurements, starting with infrared measurements made by the Explorer VII satellite (Suomi, 1958). A new three-satellite experiment, the Earth Radiation Budget Experiment (ERBE), is scheduled for a first launch in 1984 (Woerner *et al.*, 1979). Justification for such multisatellite programs rests on their ability to provide better and more accurate spatial and temporal coverage than previously available. The ERBE will use both Sun-synchronous and precessing orbits, and it will use more sophisticated data analysis algorithms and instruments than previous radiation budget experiments.

Every satellite system for measuring radiation parameters has several potential error sources, ranging from uncertainties in the merging of telemetry and ephemeris data to differing interpretations of global estimates in combination with other satellites and instruments. Errors in regional temporal averaging arise from using imperfect interpolation algorithms to infer monthly averaged regional radiant exitance from data that are temporally sparse. The inputs to this regional averaging process are spacecraft instrument measurements that have been inverted to radiant exitance at the top of the atmosphere. Such values are themselves the result of considerable mathematical manipulation and contain errors arising from bias, random and modeling sources (Green, 1983). This analysis examines the results of monthly averaging of regional measurements that are assumed to be ideal, and does not consider the errors associated with individual data inversions.

2. The nature of the temporal averaging problem

Earlier satellite experiments for measuring the Earth's radiation balance were performed on the TIROS (Bandeen *et al.*, 1965), Nimbus (Raschke and Bandeen, 1970; Jacobowitz *et al.*, 1979), and NOAA (Gruber and Winston, 1978) series. In each of these experiments, attempts have been made to infer global or "quasi-global" averages of radiation parameters from limited measurements by making various simplifying assumptions about diurnal variability. However, because of sampling restrictions, no single satellite produces enough data to define global or regional diurnal behavior in a realistic way. The Sun-synchronous (SS) Nimbus and NOAA spacecraft are restricted to coverage at fixed local times (11:30 a.m. and 8:50 a.m. on the ascending node at the equator, respectively).

The early TIROS orbits at inclinations of 48° and 58° (Rados, 1967) precessed through all local times in about 33 and 38 days, respectively, but their inability to provide uniform temporal sampling over a variety of surfaces in a shorter time complicated the inference of regional or quasiglobal averages over their areas of coverage.

This study provides a quantification of the errors associated with estimating regional monthly net radiant exitance from limited satellite samples. The sampling simulations are based on data from up to 3 satellites, each of which carries the same instruments: two in SS orbits (one each for early morning and afternoon coverage) and a third in a 57° orbit that precesses through 24 h of local time in about 37 days over those parts of the Earth available for coverage from this inclination. The SS orbits represent spacecraft in the NOAA series, while the 57° orbit is identical to that of the Earth Radiation Budget Satellite (ERBS) (Woerner *et al.*, 1979). The simulation also includes results of sampling at a series of single local hours, which represents an idealization of sampling from single SS satellites. Because a specific set of orbits has been chosen according to the requirements of the ERBE, and because of the sensitivity of the results to such choices, this study is not a simulation of a general satellite system, nor of a system that has been optimized for reducing the types of error studied.

The analysis defines regions over the grid system adopted by Minnis and Harrison (1984a) for their analysis of data from the eastern Geostationary Operational Environmental Satellite (GOES). The regions range in size from 2.50° (latitude) × 2.25° (longitude) near the Equator to 2.5° × 3.00° at ±45° latitude (Brooks, 1981). A typical distribution of sampling data from three spacecraft for an equatorial region is shown in Fig. 1. The hour index from 1 to 24 represents local solar times from 0 h 30 min to 23 h 30 min. Both of the nominal SS orbits have been used. Because the 57° orbit precesses in local time, and because the exact launch time for such an orbit is generally not known in advance, the temporal coverage for this orbit is only representative for this region. The spread in time of measurements across two or three local hours is due to the scanning mode assumed for the instrument. Note that many of the data from the 57° orbit overlap the SS coverage. Although this duplication could conceivably be used to improve confidence in individual measurements, it was assumed for this simulation that duplicated measurements provide no more information than single ones.

It is apparent from Fig. 1 that, even with the maximum assumed coverage, most of the day–hour boxes will remain empty. Since operational constraints (on the ERBE, for example) may prevent continuous availability of data from all three satellites, the situation in Fig. 1 must be assumed to be a best case for data analysis. To arrive at daily averages from a sampling

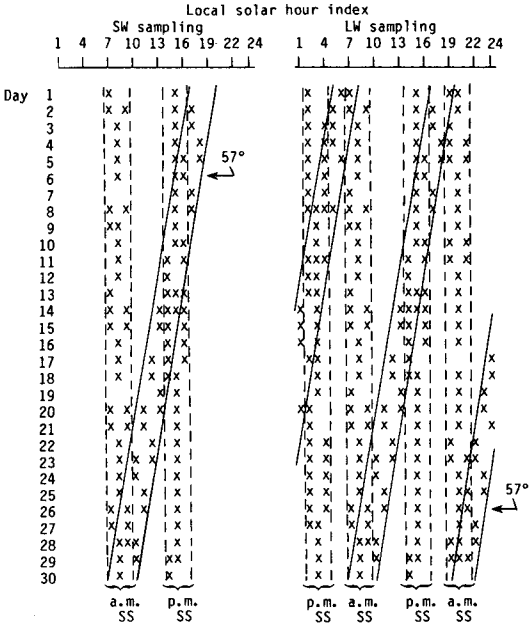

FIG. 1. Distribution of typical three-satellite samples over a near-equatorial GOES region.

situation, such as shown in Fig. 1, it is necessary to integrate radiation parameters over the day. This is done by approximating integrated values with their sums over 24 h; the missing hours are extrapolated or interpolated from existing data. Modeling of parameters at times for which the radiative behavior and meteorology are unknown is the source of temporal averaging error. Shortwave (SW) and longwave (LW) radiation parameters are analyzed separately. The Sun-driven SW diurnal variability is very prominent. The LW variability is much less pronounced, but may still be seen clearly in land regions with persistent nighttime cooling trends (Brooks and Minnis, 1984).

The contribution to solar diurnal variability in SW parameters due to the Earth's rotation and the Sun's seasonal motion is easily accounted for by standard astronomical calculations. The radiative behavior of various surface types as a function of solar zenith angle has been cataloged on the basis of previous satellite measurements, and may be supplemented with ground-based measurements or theory where necessary. The resulting models may be used to predict diurnal behavior when they are calibrated with one or more measurements over a fixed scene. However, a major contributor to diurnal variability is changing meteorology. Such changes influence a number of ground parameters that modify radiative behavior, e.g., soil moisture and sea surface roughness, but these are secondary compared to the changes in cloudiness that accompany weather patterns. The high albedo of clouds compared to surfaces other than ice or snow means that cloud variability can be a large contributor to diurnal vari-

ability in reflected SW radiation. A mathematical framework for treating SW and LW data in the context of temporally sparse sampling and variable cloud cover over land and water is given in the next section.

3. A model for regional monthly estimates of the Earth's radiation budget

The earth–atmosphere system is in approximate radiative balance with the energy input it receives from the sun. Hence, the global yearly net radiation leaving the earth must be very near zero. However, over shorter time periods and areas of the earth, the net radiant exitance can have values on the order of ± 100 W m^{-2}. The "measurements" that serve as input to modeling of this monthly net value are regional estimates of SW and LW radiant exitances, M_{SW} and M_{LW}. They represent unweighted spatial averaging of many narrow-field-of-view measurements within the region, over a time that is short compared to 1 h, and they are assumed to be unbiased with zero variance.

For the LW case, M_{LW} is taken to represent the average behavior of the region for the day–hour box into which the measurement falls. The situation for M_{SW} is more complicated. The region is assumed to be composed of different surface types, each having different time-varying albedos. For this study, three different scene types are considered: land, ocean and clouds. Their directional functions have been derived by Minnis and Harrison (1984c) from GOES data for November 1978. Table 1 gives directional reflectance δ_i as a function of μ, where $\mu(t)$ is defined in terms of the solar zenith angle ξ:

$$\mu(t) = \begin{cases} \cos\xi(t), & 0° \leqslant \xi \leqslant 90° \\ 0, & \xi > 90°. \end{cases} \tag{1}$$

Linear interpolation is used between tabulated values of μ, and the first and last tabulated values are assigned for $\mu < 0.05$ and $\mu > 0.95$. For a measurement at time t, each scene type contributes linearly to M_{SW}:

TABLE 1. Normalized directional reflectance models for three surface types.

Cosine of solar zenith angle	Model value for: Ocean	Land	Cloud
0.05	4.37	2.37	1.76
0.15	4.37	2.37	1.76
0.25	3.03	1.92	1.66
0.35	2.29	1.59	1.50
0.45	1.89	1.39	1.36
0.55	1.56	1.24	1.25
0.65	1.34	1.15	1.17
0.75	1.21	1.09	1.11
0.85	1.12	1.03	1.05
0.95	1.02	1.01	1.00

$$M_{SW}(t) = E_0(t)\mu(t) \sum_{i=1}^{N} \alpha_i(t) f_i(t). \tag{2}$$

The distance-corrected solar constant $E_0(t)$ ranges from 1331.2 to 1423.2 W m^{-2} with a value at 1 astronomical unit (AU) of 1376 W m^{-2}. Its yearly variation is very slow compared to the diurnal solar cycle; thus it is sufficient to assign one value of E_0 for each day of the year, which is calculated from the Earth–Sun distance at 0 h 0 min 0 s UT. The dimensionless quantities $\alpha_i(t)$ and $f_i(t)$ are the individual albedos and fractions ($\Sigma f_i = 1$) of N different scene types within the region.

The diurnal variation of incoming solar radiation is so pronounced that it is not a good assumption to consider all measurements of M_{SW} in an hour box as equivalent. Instead, some standard time must be selected for each hour box, and the measured values adjusted to it. The local solar time half hour has been chosen as a matter of convenience; it reflects the fact that the solar zenith angle varies symmetrically about local solar noon. Local solar time may always be approximated with sufficient accuracy by calculating local clock time from the Universal Time (UT) of the measurement and the center longitude of the region. The adjustment of $M_{SW}(t)$ to any other time t' requires knowledge of the time variation of both albedo and scene fraction:

$$M_{SW}(t') = E_0(d)\mu(t') \sum_{i=1}^{N} \alpha_i(t') f_i(t'), \tag{3}$$

where $E_0(d)$ is the distance-corrected solar constant for the day in question. At this point in the analysis, three major assumptions are made. The first is that the scene fractions are accurately known or can be calculated at the time the original spacecraft data are processed to produced the SW radiant exitance. The implications of error propagation due to systematic or random scene misidentification are beyond the scope of this study. The second assumption is that the scene fractions at time t' are the same as those at time t:

$$f_i(t') = f_i(t). \tag{4}$$

The third assumption is that the variation of albedo with solar zenith angle is known in terms of its variation with respect to a reference value at zero solar zenith angle (overhead sun):

$$\alpha_i(\mu(t')) \equiv \alpha_i(\mu = 1)\delta_i(\mu(t')), \tag{5a}$$

$$\alpha_i(\mu(t)) \equiv \alpha_i(\mu = 1)\delta_i(\mu(t)). \tag{5b}$$

Combining (5a) and (5b) yields

$$\alpha_i(\mu(t')) = \alpha_i(\mu(t))\delta_i(\mu(t'))/\delta_i(\mu(t)), \tag{6}$$

where $\delta_i(\mu)$ is the normalized directional function for scene type i. It is expected that the effects associated with the first and third assumptions will, in general, be small compared to those of the second.

Given a set of N normalized directional functions, the SW radiant exitance at time t' can be obtained in terms of known quantities at the time of observation t_{obs}:

$$M_{SW}(t') = E_0(d)\mu(t') \sum_{i=1}^{N} \alpha_i(\mu(t_{obs})) \times \delta_i(\mu(t'))f_i(t_{obs})/\delta_i(\mu(t_{obs})). \quad (7)$$

When the SW radiant exitance is adjusted to a standard time, t' is taken to be the local solar half hour.

An estimate of M_{SW} at hour h from an adjusted M_{SW} at hour h_{obs} is given by an equation with the same form as (7):

$$M_{SW}(h, h_{obs}) = E_0(d)\mu(h) \sum_{i=1}^{N} \alpha_i(\mu_{obs})\delta_i(\mu_h)f_i(t_{obs})/\delta_i(\mu_{obs}). \quad (8)$$

Suppose that measurements are available in hour boxes 6 and 12. The modeled values of SW radiant exitance for hours 7 to 11 are then time-weighted combinations of the extrapolated values from hours 6 and 12. In general, for measurements observed at hours h_1 and h_2, let

$$M_{SW}(h, h_1) = E_0(d)\mu(h) \sum_{i=1}^{N} \alpha_i(\mu_{h_1})\delta_i(\mu_h)f_i(t_{h_1})/\delta_i(\mu_{h_1}), \quad (9a)$$

$$M_{SW}(h, h_2) = E_0(d)\mu(h) \sum_{i=1}^{N} \alpha_i(\mu_{h_2})\delta_i(\mu_h)f_i(t_{h_2})/\delta_i(\mu_{h_2}). \quad (9b)$$

Then let

$$M_{SW}(h) = [(h_2 - h)M_{SW}(h, h_1) + (h - h_1)M_{SW}(h, h_2)]/(h_2 - h_1). \quad (10)$$

This weighting assumes that the scene fractions observed at h_1 change linearly to those observed at h_2. When more than one measurement is available, this weighting will almost always be an improvement over the assumption of constant meteorology for an entire day.

There is no specific diurnal model for LW radiant exitance in this study. For monthly averaging of this parameter, all of the available values for a given month are taken together. The first and last values are extrapolated as constants to the beginning and end of the month and linear interpolation is used for other missing hours. Then, the resulting month-long data record can then be divided into daily summaries as needed.

Once hourly radiation parameters are filled in for the entire day, the daily averages $\bar{M}_d(j)$ can be calculated. For either SW or LW, on day j,

$$\bar{M}_d(j) \equiv \sum_{i=1}^{24} M_{i,j}/24. \quad (11)$$

A similar calculation is used to calculate monthly averages $\bar{M}_h(i)$ for each local solar half-hour:

$$\bar{M}_h(i) \equiv \sum_{j=1}^{D} M_{i,j}/D, \quad (12)$$

where D is the number of days in the month.

The final quantity of interest is the monthly net radiant exitance. This is obtained by first defining monthly average albedo as the monthly total reflected SW radiation divided by the total incoming solar radiation:

$$\bar{\alpha} \equiv \sum_{i=1}^{24}\sum_{j=1}^{D} M_{SW}(i, j)/S, \quad (13)$$

where

$$S \equiv \sum_{i=1}^{24}\sum_{j=1}^{D} E_0(j)\mu_{i,j}. \quad (14)$$

Then define the monthly total longwave radiant exitance L_{LW}:

$$L_{LW} \equiv \sum_{i=1}^{24}\sum_{j=1}^{D} M_{LW}(i, j). \quad (15)$$

Finally, the average monthly net radiant exitance X_{net} is defined as:

$$X_{net} \equiv [(1 - \bar{\alpha})S - L_{LW}]/24D. \quad (16)$$

4. A data set for simulation of ERBE sampling

The sampling problem for ERBE data analysis would not exist if space views of the entire globe were available 24 h a day. Some regions of the Earth do, in fact, have such coverage. The eastern GOES, centered at 75°W, covers latitudes from 60°N to 60°. The coverage area used for this study encompasses latitudes from 45°N to 45°S and is shown in Fig. 2. This satellite system provides continuous data at a visible (SW) resolution of 1 km and an infrared (LW) resolution of 8 km. Scene fractions and SW and LW radiation parameters were derived from this spacecraft for November 1978 by Minnis and Harrison (1984a,c). These GOES-derived data form a realistic radiation field which can be sampled and processed with the algorithms described in the previous section.

5. Sampling strategy for simulations

Several different orbits have been used to generate simulated satellite-derived data sets from the complete GOES data set. The narrowband measurements from GOES have been converted to broadband longwave and shortwave radiant exitance following the methods used by Minnis and Harrison (1984a,c). Two SS orbits, at 7:30 a.m. (descending node) and 2:30 p.m. (as-

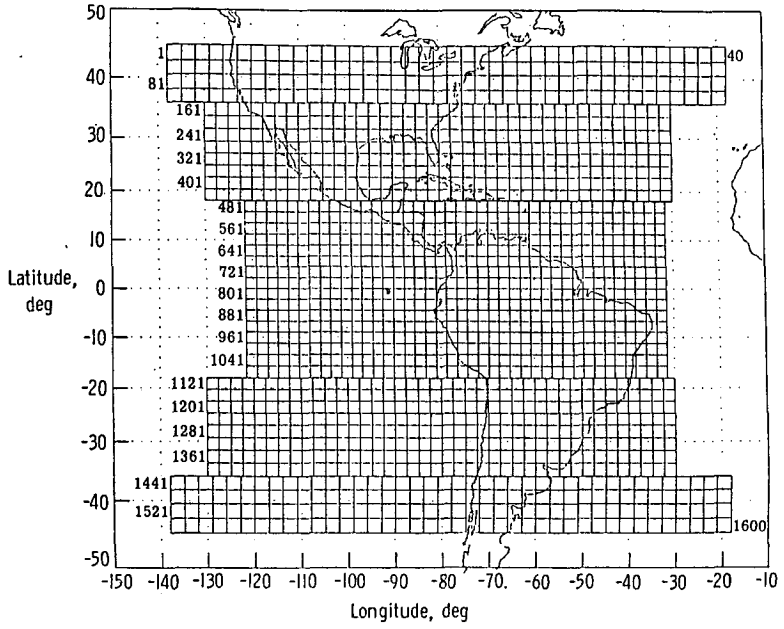

FIG. 2. Distribution of 1600 GOES regions.

cending node), and that of the 57° orbit have been used singly and in combinations. The area within the GOES field of view has been sampled in two sets of 40 regions each. One set was chosen randomly and the other was chosen by applying specific criteria as discussed below.

A monthly matrix of day and local hour coverage is generated for orbit-driven sampling over each region being studied. (The day–hour matrix in Fig. 1 is the coverage matrix for a three-satellite combination over GOES region 812.) The local time coverage of each orbit is determined by its initial orientation and subsequent nodal precession (Brooks, 1977). The contents of this sampling matrix are used to select measurements from the complete GOES data for the region. For random sampling, each of the 40 randomly selected regions has been sampled 30 times each day for 30 days. The random samples are taken in a particular way: each consists of a SW–LW measurement pair at a randomly chosen daylight hour, followed by a LW measurement 12 h later. This scheme is defined as an "ideal single sample" (ISS). It approximates the behavior of a nadir-viewing satellite and can be thought of as an idealization of sampling from a precessing orbit, which cannot be achieved in practice because of the nonrandom and slowly varying satellite–Sun geometry. If the ISS is applied to a single hour throughout the month, it is an idealization of nadir-viewing SS satellite behavior, neglecting seasonal solar motion. This scheme has been used to examine sampling errors as a function of time of measurement. The justification for defining the ISS is that it maximizes dependence on the constant meteorology assumption expressed in (4), i.e., each day's calculated reflected radiation is based on only one SW measurement. Real single satellites should produce larger errors than the 30 random samples because their sampling is never random with

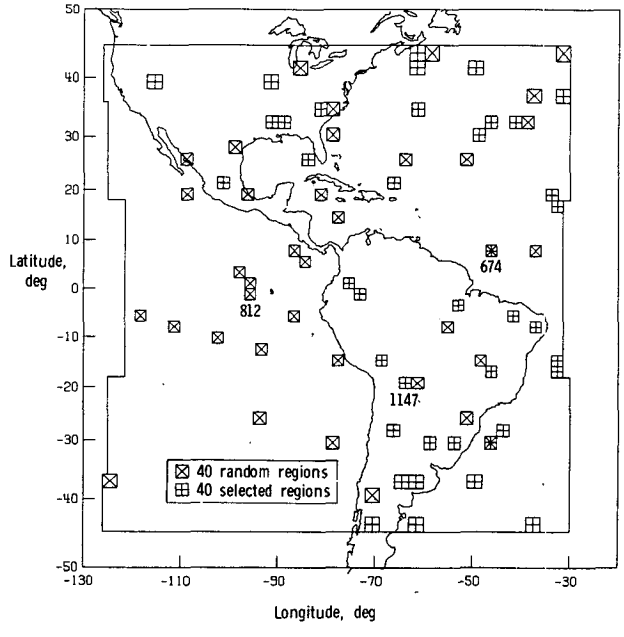

FIG. 3. Distribution of two 40-region subsets of the GOES field of view. One subset contains randomly selected regions, and the other contains 40 regions selected so that the monthly hourly average cloud fraction is nearly independent of local time. Three regions that are discussed individually in the text are identified (674, 812, 1147).

respect to time and, of course, they cannot repeat measurements at the same place and time.

6. Simulation results

The distribution of the 40 randomly chosen regions is shown in Fig. 3. This includes 30 water, 6 land, and 4 mixed (coastal) regions. The simulation results are summarized in Table 2. The basic quantity of interest in each case is the monthly net radiant exitance as defined in (16). The reference value of X_{net} is calculated for each region from the complete GOES data set, using the sums defined in (13)–(15). The missing hours resulting from various satellite sampling combinations are filled in with the models described previously; X_{net} is then calculated just as it is for the reference data. For this simulation study there is at least one measurement opportunity per day for both SW and LW, so there are no problems arising from missing days in the satellite data record.

For each sampling strategy the following quantities are also calculated: the mean algebraic difference relative to the reference value, the mean of the absolute value of the differences, minimum and maximum differences, standard estimate of the error, and standard deviation. The algebraic mean m, standard error of estimate ϵ, and standard deviation s are related by $\epsilon^2 = m^2 + s^2$. For the random sample, standard deviations may be calculated for the estimate of each region's mean, based on the 30 monthly samples. The average regional value of 4.5 W m^{-2} is expected to be larger than the standard deviation for the set of regions.

The first results given in Table 2 are for the 30 random ISSs. The algebraic mean of 1.0 W m^{-2} may be compared to the absolute mean (i.e., the average of the absolute values of the reference value of X_{net} minus the sampled value), which is 1.7 W m^{-2}. If the algebraic mean is relatively small, the qualitative explanation is that the sampled mean is relatively free from systematic bias. Application of a goodness-of-fit

TABLE 2. Summary of simulated retrievals of monthly net radiant exitance from 40 randomly selected GOES regions for various satellite sampling conditions.

	Bias in X_{net} (W m^{-2})					
Sample type	Mean	Absolute mean	Minimum	Maximum	s (W m^{-2})	ϵ (W m^{-2})
30 random ISSs	0.96	1.73	−4.2	4.6	2.00	2.21
57° @ 0 h	0.86	4.18	−16.1	10.1	5.51	5.64
6 h	−1.89	3.81	−13.9	10.1	4.47	4.85
12 h	1.29	4.96	−21.2	19.7	7.13	7.25
18 h	1.11	3.86	−7.3	11.9	4.51	4.65
a.m. SS	9.74	13.97	−14.9	47.1	16.24	18.94
p.m. SS	−4.15	6.22	−32.6	11.9	8.67	9.61
ISS @ 7:30	10.32	14.28	−17.5	49.5	16.30	19.30
8:30	8.26	10.17	−9.4	40.6	11.74	14.29
9:30	4.15	5.96	−7.6	30.3	7.96	8.98
10:30	0.38	4.07	−11.5	13.4	5.27	5.29
11:30	−0.70	5.16	−12.8	13.3	6.25	6.29
12:30	−1.93	6.28	−15.7	20.6	7.86	8.09
13:30	−3.30	6.45	−24.5	16.2	8.43	9.05
14:30	−4.98	7.47	−36.3	14.4	9.52	10.74
15:30	−4.70	7.25	−32.7	12.4	8.42	9.64
16:30	−4.43	8.16	−24.7	12.6	9.44	10.42
17:30	−6.66	9.39	−34.8	13.5	11.46	13.26
a.m. + p.m. SS	1.32	2.63	−4.0	9.4	3.17	3.44
a.m. SS + 57° @ 0 h	3.18	5.48	−10.2	19.4	6.56	7.29
6 h	2.85	4.47	−9.7	14.1	4.91	5.68
12 h	4.37	7.81	−15.5	27.7	10.02	10.93
18 h	2.54	4.81	−8.9	14.4	5.39	5.96
p.m. SS + 57° @ 0 h	−1.02	2.55	−9.8	7.6	3.34	3.49
6 h	−2.98	4.26	−21.4	8.1	5.98	6.68
12 h	−1.78	2.96	−17.2	7.1	4.17	4.53
18 h	−2.07	3.40	−18.3	6.6	4.97	5.38
Both SS + 57° @ 0 h	0.90	1.65	−2.4	5.0	1.93	2.13
6 h	0.99	1.78	−3.5	6.3	2.27	2.48
12 h	0.89	2.18	−3.7	7.8	2.67	2.82
18 h	0.66	1.48	−3.9	5.9	1.89	2.00

test, such as the Kolmogorov–Smirnoff statistic, demonstrates quantitatively that this is a reasonable conclusion for the random samples, but not for all other cases in Table 2.

The next set of data in Table 2 shows results for the spacecraft at an inclination of 57°. Its launch time is not fixed, so for all practical purposes its temporal sampling of a given region is totally unspecified at present. Hence, four different orbit plane orientations have been investigated, as specified by four different initial orbit launch times. (The launch time is not related in any obvious way to orbit orientation during the measurements.) Each orientation gives a different bias, ranging from -1.9 to 1.3 W m^{-2}, and standard deviation, ranging from 4.5 to 7.1 W m^{-2}. This leads to the conclusion that the temporal distribution of measurements determines the size and type of sampling errors. This conclusion is more obvious when SS orbits are examined. In this case, all the measurements are clustered closely around a predetermined local time. The results for early morning (0730) and early afternoon (1430) SS orbits indicate a strong dependence of mean difference on local time. The argument for larger (in magnitude) biases with morning orbits is that morning cloud cover is, in general, much less representative of daily average meteorology than midday cloud cover. A large positive bias in the morning means that the algorithms hve underestimated net radiant exitance. One explanation for this is that generally higher morning cloud cover produces an overestimate of average albedo, leading to an underestimate of net radiation [see Eq. (15)]. The standard deviation of a.m. SS measurements is also relatively high, yielding a value of ϵ which is twice that of the p.m. SS orbit.

Selected closer examinations of these regions (in an unpublished study by the authors) hve shown that the values of ϵ for monthly mean LW radiant exitance are -0.4 and 0.5 W m^{-2} for the p.m. SS and 57° orbits (at a launch time of 12 h), respectively. Thus, the biases and random errors shown here for these regions appear to be due almost entirely to the difficulty of retrieving SW diurnal behavior from sparse satellite sampling. (In a set of 40 land regions with high LW variability studied previously by Brooks and Minnis (1984), ϵ values for monthly net radiant exitance of 6.5 and 9.0 W m^{-2} were observed for the same p.m. SS and 57° orbits. The corresponding ϵ values for LW radiant exitance were 3.6 and 5.6 W m^{-2}, which demonstrated that LW diurnal variability can be a significant error source in some regions. More accurate methods of modeling LW behavior are available, but are not necessary for this simulation.)

The series of ISSs shown in Table 2 for local daylight hours from 0730 to 1730 verifies the strong dependence of monthly net bias on time of measurement. The algebraic mean difference varies from the largest positive value of 10.3 W m^{-2} in the early morning to a negative value of -6.7 W m^{-2} in the late afternoon. This effect will be examined in more detail below. The 0730 ISS corresponds roughly to the 1930 a.m. SS orbit. The ISS mean bias is a little higher than for the SS orbit because the actual orbit simulation allows a small spread in local times of measurement, as shown in Fig. 1. Note also that by the same argument, the 1130 ISS corresponds to a Nimbus-type orbit. All other things being equal, this allows assignment of a temporal sampling-induced bias of substantially less than 1 W m^{-2} in monthly net radiant exitance for data taken in such orbits. Care must be taken if these results are extrapolated to regions outside the GOES field of view, where the local time of an SS measurement may differ substantially from its Equator-crossing time.

The next results in Table 2 are for various satellite combinations. Together, the a.m. and p.m. SS satellites produce monthly nets that have a very low algebraic mean difference. However, these simulations assume that all spacecraft data are equivalent whereas it is generally recognized, for example, that inversions of early morning (or late afternoon) measurements from satellite altitude to the top of the atmosphere are much less accurate than inversions done at higher solar elevation angles. It should be emphasized that the errors given in Table 2 arise only from differences in temporal sampling, and do not include errors from other sources. Four different launch timings for the 57° orbit in conjunction with an a.m. SS orbit yield standard errors of estimate between about 6 and 11 W m^{-2}, and the same estimates with the p.m. SS orbit lie between about 3 and 7 W m^{-2}. The relatively high error associated with the early morning orbit indicates again that early afternoon SS orbits are a much better choice for Earth radiation monitoring. (The early a.m. SS orbits are included in these simulations because they represent vehicles of opportunity for ERBE instruments.)

As expected, a combination of three satellites gives the smallest biases, with standard errors of estimate between about 2 and 3 W m^{-2}. In this case, more complete sampling of the diurnal cycle minimizes modeling errors. The constant meteorology assumption is effectively replaced with the assumption that meteorology changes linearly between one measurement and the next.

It is of interest to determine the nature of the time-dependent biases in X_{net} obtained when ISSs are generated at a series of local hours. Since these cases invoke the constant meteorology assumption for an entire day, the most obvious explanation of the resulting biases is that meteorological conditions exhibit a related, monthly averaged, time-dependent behavior over the area encompassed by the set of 40 regions. For our purposes, meteorology essentially means total cloud cover as viewed from a satellite. This parameter is available from the GOES data as one of the inputs to the net radiation calculations.

Since it is unlikely that global radiation monitoring will be done in the near future with diurnally complete, concurrent cloud information, the GOES hourly cloud data have been compressed into monthly averages of cloud fractions at each hour. Such data may eventually be available on a global basis and could be compiled into a regionally resolved, monthly averaged, seasonally dependent, global cloud model that could be used in the interpretation of satellite-derived Earth radiation measurements. The mean errors for the ISSs shown in Table 2 are plotted in Fig. 4a as a function of hour box index (an "8" is 0730, local solar time) along with the monthly hourly average (mha) total cloud fraction. The trend from higher to lower cloud cover from morning to afternoon seems qualitative confirmation of the relationship between meteorology and bias from time-localized measurements.

To further investigate this relationship, another set of 40 GOES regions was selected. Their distribution is shown in Fig. 3. These regions were chosen such that, taken together, they have an mha cloud cover

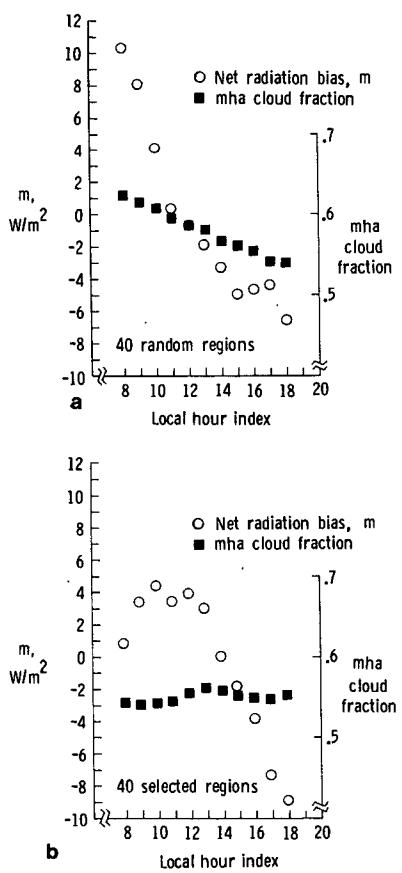

FIG. 4. Monthly average bias in net radiant exitance resulting from sampling at single hours, and monthly hourly cloud fraction as a function of local hour index for (a) 40 randomly chosen GOES regions and (b) 40 GOES regions with cloud fraction nearly independent of local time.

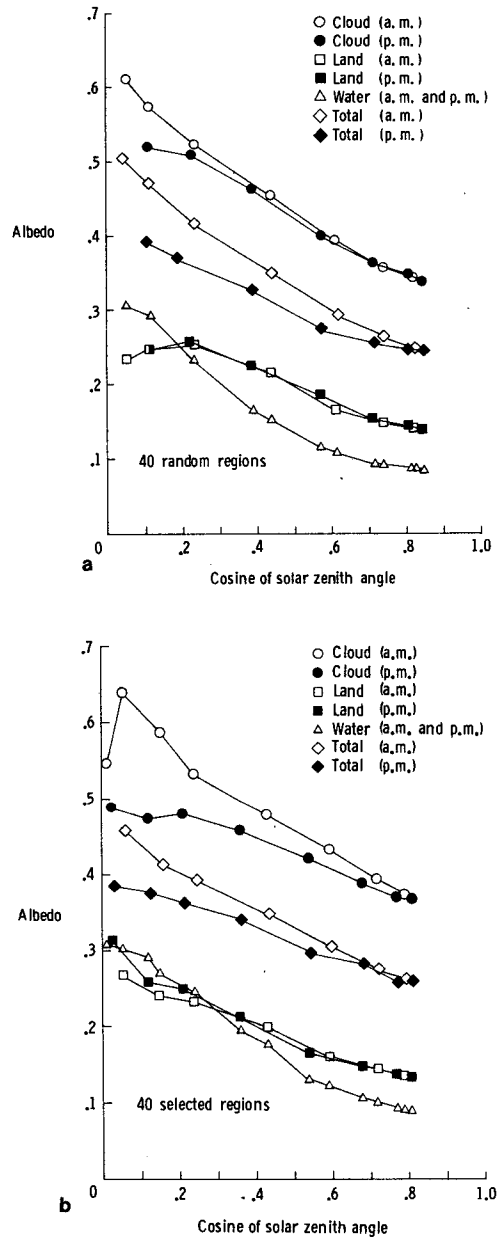

FIG. 5. Scene and total albedos as a function of cosine of the solar zenith angle for (a) 40 randomly chosen GOES regions and (b) GOES regions with cloud fraction nearly independent of local time.

which is essentially independent of local time. The Pacific is excluded from this set because of the predominant diurnal behavior observed there (see Minnis and Harrison, 1984b). The mean bias errors resulting from ISSs taken at hour indices from 8 to 18 are plotted along with mha cloud cover in Fig. 4b. Note that while the biases are smaller for these specially selected regions than for the original 40 randomly chosen regions, the same morning to afternoon trend is observed. This

effect can be explained by examining the mha albedos rather than the cloud fraction. The mha land, water, cloud, and total albedos are shown as a function of the cosine of the solar zenith angle in Fig. 5 for both sets of 40 regions. Morning and afternoon values for land, cloud, and total albedos are distinguished by open and filled symbols. (Water albedo was assumed to be symmetrical about local solar noon in the GOES analysis.) The significant point is that total albedo in each case is not symmetrical about local solar noon, but is higher in the morning than in the afternoon. The asymmetry is due in each case to the assigned albedo and distribution of clouds. In the 40 random regions, the asymmetry is due mainly to the mha diurnal variability in cloud fraction. In the second set of regions, where the cloud shows, on the average, little diurnal variability, the asymmetry is due mostly to diurnal variability in cloud albedo.

Some insight into the explanation for these results can be obtained by examining individual GOES regions. Three regions with different behavior are examined in Figs. 6 and 7. Their locations within the GOES field of view are shown in Fig. 3. Region 812 lies just south of the equator off the coast of Ecuador. It exhibits the persistent strong diurnal cloud variability typical of this part of the Pacific. The mean biases obtained with ISSs, and the mha cloud cover are shown in Fig. 6(a). The bias in net radiant exitance is strongly positive in the morning and negative in the afternoon. The water, cloud, and total albedos for this region are shown in Fig. 7a. Region 674 lies in the western Atlantic off the coast of Brazil, within the Intertropical Convergence Zone. Its biases and albedos are shown in Figs. 6b and 7b. In this part of the Atlantic, the time of maximum cloudiness varies considerably from region to region. In 674, maximum cloudiness occurs in the early afternoon; thus the bias in net radiant exitance is negative in the morning and positive in the afternoon.

The differences between cloud properties of region 812 and 674 are readily apparent from a comparison of Figs. 6a and 6b, and 7a and 7b. In 812, the cloud albedos shown in Fig. 7a are nearly symmetric about local noon. Clouds in this region are mostly low-level stratocumulus and show very little diurnal change in vertical structure (Minnis and Harrison, 1984b). The morning–afternoon asymmetry observed in total albedo is due almost entirely to persistent higher morning cloud amounts. In 674, the total albedo as shown in Fig. 7b is lower in the morning than in the afternoon. This difference is explained partly by smaller morning cloud fractions, but also by lower morning cloud albedo, indicating that the physical properties of morning and afternoon clouds differ significantly in this region

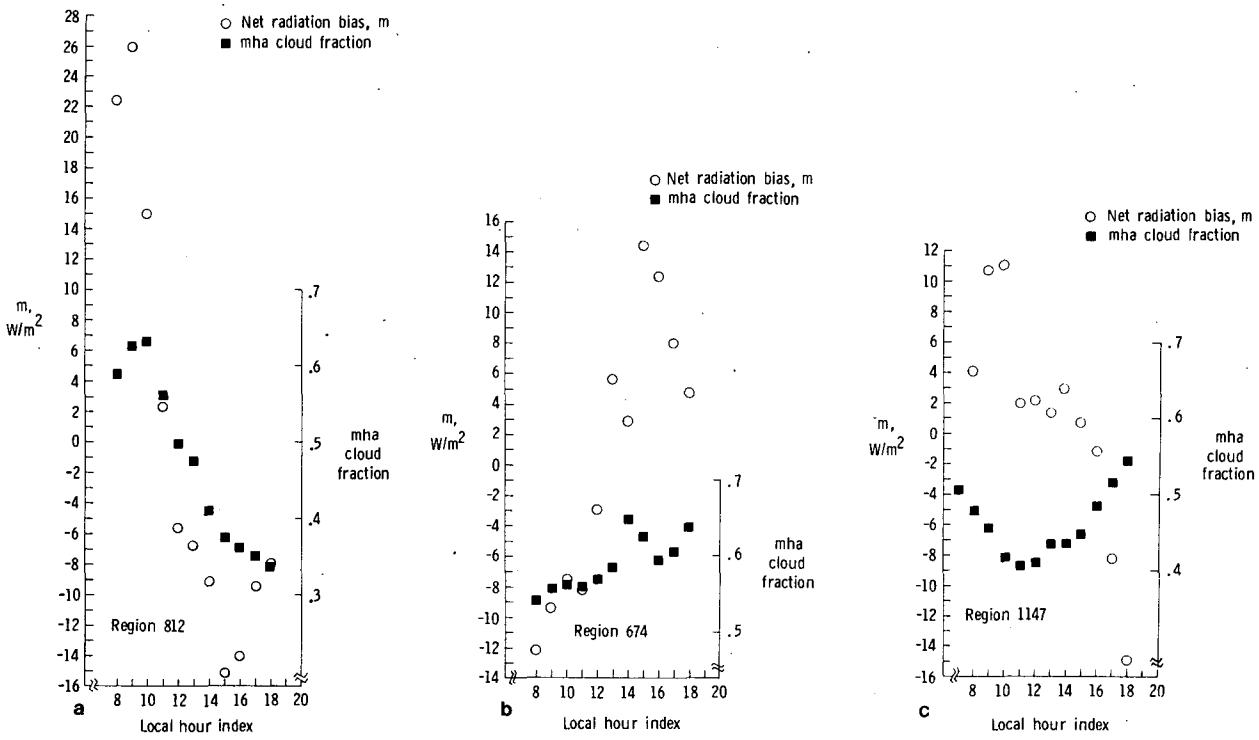

FIG. 6. Monthly average bias in net radiant exitance from sampling at single hours, and monthly hourly cloud fraction as a function of local hour index for GOES region: (a) 812, (b) 674, (c) 1147.

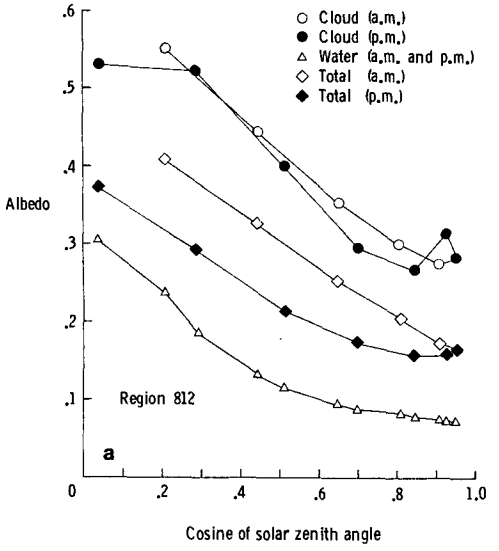

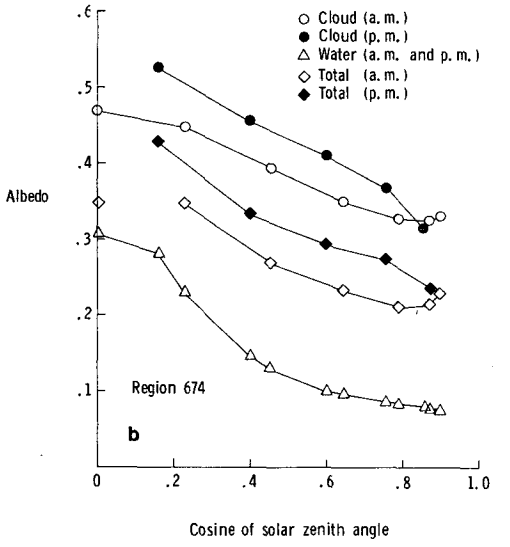

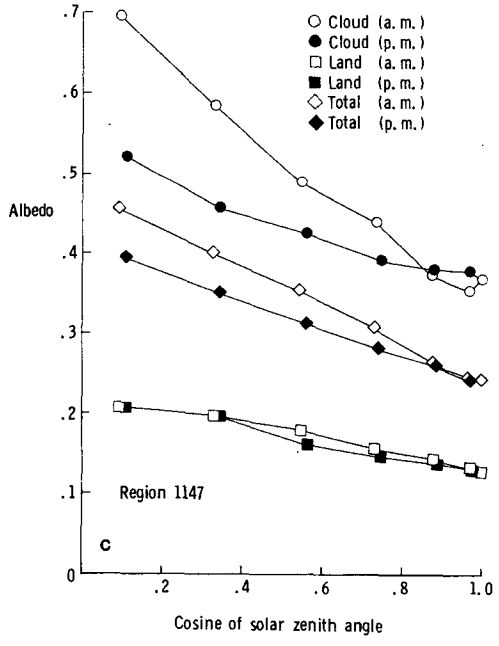

FIG. 7. Scene and total albedos as a function of cosine of the solar zenith angle for GOES region: (a) 812, (b) 674, (c) 1147.

and season. Examination of the average vertical distribution of clouds for this region reveals that upper and middle level cloudiness is more prevalent in the morning than in the afternoon.

Region 1147 is in Bolivia on the east slope of the Andes. Unlike the other two regions, the biases observed for 1147 (shown as a function of local hour in Fig. 6c) bear little apparent relationship to cloud fraction variability. The albedo behavior shown in Fig. 7c indicates substantial morning–afternoon differences in cloud structure. Here, the afternoon increase in high cloudiness appears to be mostly in the form of a low-albedo cirrus shield. The complexity of this region is also due to strong diurnal longwave variability. The net bias depends on the individual monthly average estimates of longwave radiant exitance and albedo, and on how they combine in (16) at a particular hour. The relatively high biases at 0900 and 1000 are due mostly to overestimates of albedo. For measurements in the late afternoon, both longwave and albedo are underestimated such that overall bias is reduced below the early a.m. values. Finally, at the last afternoon

hour, the albedo estimate is so low that it overwhelms the longwave underestimate, leading to a large negative bias.

7. Concluding remarks

The simulation results presented in the previous section show that single-satellite measurements produce complex systematic biases in a monthly regional averaging process. The biases are traced to an inability to extract the asymmetry of cloud amount and albedo from measurements at or clustered about a single local solar time. Additional possible sources of bias include scene identification and directional modeling errors. These are ignored for the present study; hence the results given in Table 2 are representative only of temporal sampling errors and not the total error expected due to a combination of scene identification, directional modeling, and other errors. Sun-synchronous satellites (and the idealized single samples used to examine the effects of measurements at a single local time) exhibit this effect most clearly. It can also be seen in results from the 57° orbit when used by itself or in conjunction with SS orbits when it happens to lie in an orientation that does not significantly supplement local time coverage from a particular SS orbit.

The three individual regions presented in detail illustrate both the general principles and the complexity of retrieving more accurate monthly net radiant exitance estimates from sparse satellite measurements. In regions with small surface longwave diurnal variability, particularly over the ocean, the qualitative relationship of cloud behavior and estimated monthly average SW or net radiant exitance can easily be seen. However, even the hindsight provided by meteorological information may not be sufficient to quantify the relative contributions of cloud amount and cloud properties because these two factors work together to modify the radiative behavior of the clear surface. In some land regions, large longwave diurnal variability can push monthly net estimates significantly in either the right or wrong direction, making the net bias even more difficult to remove without detailed meteorological knowledge of the regions.

The results presented here are in good agreement with those of Minnis and Harrison (1984c). Their study used monthly average values to examine monthly net radiant exitance, rather than relying on actual diurnal modeling to obtain daily averages. Such an approach differs very little in practice from the present one when applied to SS orbits, but is less applicable to processing orbits, or to multiple orbits. A more general study of sampling requirements for multisatellite missions was conducted by Harrison *et. al.* (1983). Their comparison of various sampling strategies was based more on geometric arguments than on a direct assessment of time–space averaging errors. Nonetheless, both the magnitude and relative size of errors associated with single and multiple satellite sampling are consistent with the present results. Further, Harrison *et. al.* (1983) showed that sampling errors are a function of latitude and are largest in the equatorial regions. This is expected, given the strong dependence of tropical meteorological processes on the daily solar cycle.

The results presented can easily be seen to depend on the regions and orbits selected. Hence, generalization of this study must proceed with caution. In addition, only November 1978 GOES data have been analyzed, and a pronounced seasonal dependence is to be expected. Even though there is no way of knowing if the largest errors observed are representative of other seasons or parts of the globe, the relative performance of various types of sampling is expected to hold over the globe and all seasons. Reduction of sampling errors for the Earth Radiation Budget Experiment below the level possible with the available orbits will require additional analysis either with specific meteorological information, contemporary satellite data, or global cloud climatology models.

This study has shown that analysis of data from a three-satellite mission like the Earth Radiation Budget Experiment can reduce both individual regional and 40-region average errors of estimate for monthly net radiant exitance by an order of magnitude over those obtained for the worst single satellite cases. The 40-region standard errors of estimate for three satellites ranged from 2 to 3 W m^{-2}, while single satellite errors ranged from 5 to 19 W m^{-2}. Representative two-satellite samples also provide significant gains over single satellites, yielding errors of estimate ranging from 3 to 11 W m^{-2}. The most likely initial multiple satellite combination available to the Earth Radiation Budget Experiment is a p.m. Sun-synchronous NOAA spacecraft and the Earth Radiation Budget Satellite at 57°. The 40-region errors of estimate from this combination range from 3 to 7 W m^{-2}.

Acknowledgments. We would like to thank Mr. Gary G. Gibson, Kentron International, Hampton Technical Center, Hampton, Virginia, for his preparation of the orbit-driven data sampling tapes used in this study, and members of the Earth Radiation Budget Experiment Science Team for their input to and discussion of the analysis algorithms presented here.

REFERENCES

Bandeen, W. R., M.. Halev and I. Strange, 1965: A radiation climatology in the visible and infrared from the Tiros Meteorological Satellites. NASA TN D2534, 30 pp. [NTIS N65-24522].

Brooks, D. R., 1977: An introduction to orbit dynamics and its application to satellite-based Earth monitoring systems NASA RP-1009, 80 pp. [NTIS N78-12113].

——, 1981: Grid systems for Earth Radiation Budget Experiment applications. NASA TM-83233, 39 pp. [NTIS N82-14818].

——, and P. Minnis, 1984: Comparison of longwave diurnal models

applied to simulations of the Earth Radiation Budget Experiment. *J. Climate. Appl. Meteor,* **23,** 155–160.

Green, R. N., 1983: Accuracy and resolution of Earth radiation budget estimates. *J. Atmos. Sci.,* **40,** 977–985.

Gruber, A., and J. S. Winston, 1978: Earth–atmosphere radiative heating based on NOAA scanning radiometer measurements. *Bull. Amer. Meteor. Soc.,* **59,** 1570–1573.

Harrison, E. F., P. Minnis and Gary G. Gibson, 1983: Orbital and cloud cover sampling analyses for multisatellite Earth radiation budget experiments. *J. Spacecr. Rockets,* **20,** 491–495.

Jacobowitz, H., W. L. Smith, H. B. Howell, F. W. Nagle and J. R. Hickey, 1979: The first 18 months of planetary radiation budget measurements from the Nimbus 6 ERB experiment. *J. Atmos. Sci.,* **36,** 508–518.

Minnis, P.,and E. F. Harrison, 1984a: Diurnal variability of regional cloud and clear sky radiative parameters derived from GOES data. Part I: Analysis method. Submitted to *J. Climate. Appl. Meteor.*

——, and ——, 1984b: Diurnal variability of regional cloud and clear sky radiative parameters derived from GOES data. Part II: November 1978 cloud distribution. Submitted to *J. Climate. Appl. Meteor.*

——, and ——, 1984c: Diurnal variability of regional cloud and clear sky radiative parameters derived from GOES data. Part III: November 1978 radiative parameters. Submitted to *J. Climate. Appl. Meteor,.*

Rados, R. M., 1967: The evolution of the TIROS meteorological satellite operational system. *Bull. Amer. Meteor. Soc.,* **48,** 326–337.

Raschke, E., and W. R. Bandeen, 1970: The radiation balance of the planet Earth from radiation measurements of the satellite Nimbus II. *J. Appl. Meteor.,* **9,** 215–238.

Suomi, V. E., 1958: The radiation balance of the Earth from a satellite. *Annals of the IGY,* Vol. 1, 331–340.

Woerner, C. V., J. E. Cooper and E. F. Harrison, 1979: The Earth radiation budget satellite system for climate research. *Advances in Space Exploration.* Vol. 4, *Remote Sounding of the Atmosphere from Space,* H.-J. Bolle, Ed., COSPAR, 201–215.